

Strange quark star in dilaton gravity

Alireza Peivand¹, Kazem Naficy¹ and Gholam Hossein Bordbar^{2,3,4}

¹ Department of Physics, University of Birjand, P.O. Box 615/97175, Birjand, South Khorasan, Iran;
naficy@birjand.ac.ir

² Department of Physics, Shiraz University, Shiraz 71454, Iran; ghbordbar@shirazu.ac.ir

³ Research Institute for Astronomy and Astrophysics of Maragha, P.O. Box 55134-441, Maragha, Iran

⁴ Department of Physics and Astronomy, University of Waterloo, 200 University Avenue West, Waterloo, Ontario, N2L3G1, Canada

Received 2018 July 5; accepted 2018 November 4

Abstract In this work, we first obtain the hydrostatic equilibrium equation in dilaton gravity. Then, we examine some of the structural characteristics of a strange quark star in dilaton gravity in the context of Einstein gravity. We show that the variations of dilaton parameter do not affect the maximum mass, but variations in the cosmological constant lead to changes in the structural characteristics of the quark star. We investigate the stability of strange quark stars by applying the MIT bag model with dilaton gravity. We also provide limiting values for the dilaton field parameter and cosmological constant. We also study the effects of dilaton gravity on the other properties of a quark star such as the mean density and gravitational redshift. We conclude that the last reported value for the cosmological constant does not affect the maximum mass of a strange quark star.

Key words: dense matter — equation of state — gravitation — stars: fundamental parameters (masses, radii)

1 INTRODUCTION

Einstein's Theory of General Relativity (GR) explains phenomena and events well within the solar system. Tolman, Oppenheimer and Volkoff (TOV) (Tolman 1939; Oppenheimer & Volkoff 1939) obtained the first hydrostatic equilibrium equation (HEE) from the solution of Einstein's field equations. So far, the structure of compact objects, such as neutron stars and quark stars that have general relativistic properties due to their great density, has been modeled by many authors through the numerical solution of the TOV equation (Silbar & Reddy 2004; Bordbar et al. 2006, 2016; Narain et al. 2006).

In recent years, studies outside the solar system have led to the emergence of new theories and observations such as accelerated expansion of the universe (Knop et al. 2003; Perlmutter et al. 1999; Riess et al. 1998; Tonry et al. 2003), which GR is incapable of explaining. The absence of a comprehensive gravitational theory on quantum scales has led to a lot of attention being focused on the emergence of new gravitational theories. Such theories include GR and

can explain new cosmological phenomena, and discoveries that GR cannot explain and interpret well.

Adding new terms, including higher-order curvature invariants and scalar fields, to Einstein Lagrangian yields theories that are known as modified gravity. One of these new modified gravities considers the dilaton scalar field and its potential in the universe. The scalar field has been used to justify inflation and also to describe cold dark matter (Cho 1990), which is a type of dark matter. Recently, study of the structure of compact objects in modified gravity has been widely considered including neutron stars (Astashenok 2016; Hendi et al. 2015), black holes (Chan et al. 1995; Hendi et al. 2016b) and quark stars (Astashenok 2016; Astashenok et al. 2015).

To obtain the structural characteristics of compact objects in the new gravities, we use the action related to the proposed gravitational theory. By varying this action and taking the principle of least action into account, we derive the field equation for the considered gravity. Then by solving this equation and using conservation of the momentum-energy tensor, we procure the HEE of the new theory.

Furthermore, by using the equation of state (EoS) of matter in the compact object, we solve the derived HEE equation numerically and yield the maximum mass and radius of the star under study. The HEE in modified gravity has been considered by several authors: HEE in Gauss-Bonnet gravity (Momeni & Myrzakulov 2015), HEE in $f(G)$ gravity (Sharif & Fatima 2016), HEE in $f(R)$ gravity (Astashenok 2016; Astashenok et al. 2013; Arapoğlu et al. 2011), HEE in gravity's rainbow (Hendi et al. 2016a) and HEE in massive gravity (Katsuragawa et al. 2016; Hendi et al. 2017).

After Witten conjectured the hypothesis of strange quark matter (Witten 1984; Farhi & Jaffe 1984), it has been shown that a new class of compact objects may exist which is composed from strange quark matter, known as strange quark stars (SQSs) or strange stars (Haensel et al. 1986; Alcock et al. 1986b,a; Alcock & Olinto 1988; Glendenning 1990). SQSs are composed from up (u), down (d) and strange (s) quarks along with a small number of electrons that are in β equilibrium. The best candidates for SQSs are some of the observed compact objects that may not be compatible with the neutron star model, such as X-ray pulsar LMC X-4 with $M = 1.29 \pm 0.05 M_{\odot}$ (Gangopadhyay et al. 2013; Paul et al. 2011; Rawls et al. 2011), X-ray burster 4U 1608-52 (Paul et al. 2011; Bombaci 1997; Dey et al. 1998) with $M = 1.74 \pm 0.14 M_{\odot}$ (Güver et al. 2010) and millisecond pulsar J1614-2230 (Paul et al. 2011; Deb et al. 2017) with $M = 1.97 \pm 0.04 M_{\odot}$ (Demorest et al. 2010). In this work, the considered quark star is made of strange quark matter from the center up close to the surface. Here, we want to calculate some bulk properties of an SQS by using the modified HEE in dilaton gravity and considering the MIT bag model to produce the EoS of strange quark matter (SQM). This paper is divided into six sections. In Section 2, we propose a new procedure to find HEE in dilaton gravity in the context of Einstein gravity. In Section 3, we present the HEE in dilaton gravity as a correction of the HEE in Einstein gravity (correction of TOV). In Section 4, we obtain the maximum mass of the quark star from the numerical solution of the HEE generated in Sections 2 and 3 and compare our results with the results obtained in GR. In Section 5, we investigate causality condition and dynamical stability of SQSs in dilaton gravity. Our conclusions are drawn in Section 6.

2 HEE IN DILATON GRAVITY

The total action of dilaton gravity (S_{total}) is as follows

$$S_{\text{total}} = \frac{1}{2\kappa} \int d^4x \sqrt{-g} \left(R - 2g^{\mu\nu} \partial_{\mu} \Phi \partial_{\nu} \Phi - V(\Phi) \right) + S_{\text{matter}}, \quad (1)$$

in which Einstein's gravity is regarded as the background. In this action, R , Φ and $V(\Phi)$ are the Ricci scalar, dilaton field and potential of this field, respectively. S_{matter} is the action related to the matter, which is considered to be a perfect fluid. To find the dilaton field equation, we vary Equation (1) with respect to the dilaton field Φ and the metric tensor $g_{\mu\nu}$. Using the principle of least action, field equations are obtained as follows

$$G_{\mu\nu} = \kappa T_{\mu\nu} + \left(2\partial_{\mu} \Phi \partial_{\nu} \Phi - g_{\mu\nu} \partial_a \Phi \partial^a \Phi - \frac{1}{2} g_{\mu\nu} V(\Phi) \right), \quad (2)$$

$$\square \Phi - \frac{1}{4} \frac{\partial V}{\partial \Phi} = 0, \quad (3)$$

where $G_{\mu\nu}$ and $\kappa = \frac{8\pi G}{c^4}$ are the Einstein tensor and Einstein gravitational constant, respectively. $T_{\mu\nu}$ is the energy-momentum tensor associated with a perfect fluid. We consider that the potential of a dilaton field consists of two Liouville terms

$$V(\Phi) = 2\Lambda_0 e^{2\xi_0 \Phi} - 2\Lambda e^{2\xi \Phi}. \quad (4)$$

Potentials of this type have been previously studied to solve dilaton black hole field equations (Chan et al. 1995; Dehghani & Farhangkhah 2005).

To find a static solution of Equations (2) and (3), we assume the four-dimensional spacetime metric as

$$ds^2 = -B(r) dt^2 + \frac{dr^2}{A(r)} + R^2(r) r^2 d\Omega^2, \quad (5)$$

in which $B(r)$, $A(r)$ and $R(r)$ are unknown functions to be determined and $d\Omega^2 = (d\theta^2 + \sin^2 \theta d\phi^2)$. We consider $R(r)$ as the ansatz which has the form

$$R(r) = e^{\alpha \Phi(r)}. \quad (6)$$

This ansatz was first used to investigate answers related to field equations of charged dilaton black strings (Dehghani & Farhangkhah 2005). Recently, this ansatz has been applied by some authors (Sheykhi et al. 2006; Hendi et al. 2015) to study properties of dilaton gravity. It is important to note that when $\alpha = 0$, the ansatz becomes $R(r) = 1$ and dilaton gravity turns to Einstein gravity. By making this ansatz and using Equation (3), and introducing the metric in Equation (5), we have

$$\Phi(r) = \frac{\alpha}{1 + \alpha^2} \ln \left(\frac{b}{r} \right), \quad (7)$$

where b is an arbitrary constant.

For a perfect fluid, the general form of energy-momentum tensor is given by

$$T^{\mu\nu} = (\rho c^2 + P) u^{\mu} u^{\nu} + P g^{\mu\nu}. \quad (8)$$

In these relations, P and ρ are the pressure and energy density of the perfect fluid from the viewpoint of the local observer respectively, and u^μ is the local fluid velocity 4-vector. Using the metric defined by Equations (5) and (8), the energy-momentum tensor for the perfect fluid has the form

$$T^a_b = \text{diag}(-\rho c^2, P, P, P). \quad (9)$$

To solve the dilaton field equation, with the metric Equation (5) and energy-momentum tensor Equation (9), we obtain the components of Equation (2) as follows

$$\kappa \rho c^2 = -\Lambda \gamma \alpha^2 - \frac{A'}{r K_{1,1}} - \frac{AK_{1,-3}}{r^2 K_{1,1}^2} + \frac{\gamma \alpha^2}{K_{-1,1} b^2} + \frac{1}{r^2 \gamma \alpha^2}, \quad (10)$$

$$\kappa P = \Lambda \gamma \alpha^2 + \frac{AB'}{r B K_{1,1}} + \frac{AK_{1,-3}}{r^2 K_{1,1}^2} - \frac{\gamma \alpha^2}{K_{-1,1} b^2} - \frac{1}{r^2 \gamma \alpha^2}, \quad (11)$$

$$\begin{aligned} \kappa P = \Lambda \gamma \alpha^2 + \frac{AB'}{2r B K_{1,1}} - \frac{2\alpha^2 A}{r^2 K_{1,1}^2} - \frac{\gamma \alpha^2}{K_{-1,1} b^2} - \frac{AB'^2}{4B^2} \\ + \frac{A'B'}{4B} + \frac{A'}{2r K_{1,1}} + \frac{AB''}{2B}, \end{aligned} \quad (12)$$

where

$$K_{i,j} \equiv i + j \alpha^2, \quad \gamma \equiv \left(\frac{b}{r} \right)^{\frac{2}{K_{1,1}}},$$

and the prime and double-prime denote the first and second derivatives with respect to r respectively. Furthermore, by using conservation of the energy-momentum tensor $T^{\mu\nu}{}_{;\mu} = 0$ we have

$$\frac{dP}{dr} = -(\rho c^2 + P) \left(\frac{B'}{B} \right). \quad (13)$$

It is notable that in Equations (10) to (12), we set Λ to be a free parameter and it behaves the same as a cosmological constant. Meanwhile, Λ_0 , ξ_0 and ξ are constants that are chosen as follows to solve Equations (2) and (3)

$$\Lambda_0 = \frac{\alpha^2}{b^2 K_{-1,1}}, \quad \xi_0 = \frac{1}{\alpha}, \quad \xi = \alpha.$$

The function $A(r)$ is obtained by integrating Equation (10) in the form

$$\begin{aligned} A(r) = \left(\frac{\gamma^{-\alpha^2}}{r^2 K_{1,-1}} - \frac{\Lambda \gamma \alpha^2}{3 K_{1,-1}} - \frac{\gamma \alpha^2}{K_{1,-1}^2 b^2} \right) r^2 K_{1,1}^2 \\ - \frac{\kappa c^2 K_{1,1}}{r^{\frac{K_{1,-3}}{K_{1,1}}}} \int r^{\frac{2K_{1,-1}}{K_{1,1}}} \rho(r) dr. \end{aligned} \quad (14)$$

If we replace $\alpha = 0$ in this equation, then we see that $A(r)$ in the dilaton field reduces to known $A(r) = \left(1 - \frac{2GM}{rc^2} -$

$\frac{\Lambda}{3} r^2$) in Einstein- Λ gravity (Stuchlík 2000; Balaguera-Antolínez et al. 2005; Böhmer & Harko 2005a), therefore, we can write $4\pi \int r^{\frac{2K_{1,-1}}{K_{1,1}}} \rho(r) dr = M_{\text{eff}}(r, \alpha)$ in which $M_{\text{eff}}(r, \alpha) = \int 4\pi \rho(r) R_{\text{eff}}^2 dR_{\text{eff}}$ is the effective mass with the corresponding effective radius that is given by $R_{\text{eff}} = \sqrt[3]{\frac{3K_{1,1}}{K_{3,-1}}} r^{\left(\frac{K_{3,-1}}{3K_{1,1}}\right)}$. One can obtain $\frac{B'}{B}$ by substituting Equation (14) into Equation (11), then replacing $\frac{B'}{B}$ in Equation (13). With this replacement and using $\frac{dP}{dr} = \frac{dP}{dR_{\text{eff}}} \frac{dR_{\text{eff}}}{dr}$, we obtain dilaton HEE as

$$\begin{aligned} \frac{dP}{dR_{\text{eff}}} = \frac{1}{2} \sigma^{\frac{4\alpha^2}{3K_{1,1}}} \delta^{-\frac{2K_{1,-1}}{K_{1,1}}} (c^2 \rho + P(r)) \\ \times \left[-\frac{\sigma \delta K_{1,1} P(r) \kappa}{\tau} - \frac{K_{1,1}}{\sigma \delta \tau Y \alpha^2} \right. \\ \left. + \frac{\sigma \delta K_{1,1} \Lambda Y \alpha^2}{\tau} + \frac{\sigma \delta K_{1,1} \alpha^2 Y}{\tau b^2 K_{1,-1}} \right. \\ \left. + \frac{K_{1,-3}}{\sigma \delta K_{1,1}} \right] \end{aligned} \quad (15)$$

with

$$\begin{aligned} \tau = \frac{K_{1,1}^2}{\Upsilon \alpha^2 K_{1,-1}} - \frac{K_{1,1}^2 \delta^2 \sigma^2 \Upsilon \alpha^2}{K_{1,-1}^2 b^2} - \frac{K_{1,1}^2 \delta^2 \sigma^2 \Lambda \Upsilon \alpha^2}{3 K_{1,-1}} \\ - \frac{\kappa c^2 K_{1,1} M_{\text{eff}}}{4\pi \left((\sigma \delta)^{\frac{K_{1,-3}}{K_{1,1}}} \right)}, \\ \Upsilon = \left(\frac{b}{\sigma \delta} \right)^{\frac{2}{K_{1,1}}}, \\ \delta = R_{\text{eff}}^{\left(\frac{3K_{1,1}}{K_{3,-1}}\right)}, \\ \sigma = \left(\frac{K_{3,-1}}{3K_{1,1}} \right)^{\left(\frac{K_{1,1}}{K_{3,-1}}\right)}. \end{aligned}$$

It is important to note that in dilaton gravity, gravitational mass, $m(r) = \int 4\pi r^2 \rho(r) dr$ and radius, r , are modified to M_{eff} and R_{eff} respectively.

3 DILATON HEE AS A CORRECTION OF TOV

In this section, we use the same techniques as in Hendi et al. (2015). We expand Equation (15) in a series of α . When α has very small values, we can neglect all terms of

order higher than 2, then we have

$$\begin{aligned}
\frac{dP}{dr} = & \frac{(4r^3 P(r) \kappa \pi - \frac{8}{3} \Lambda \pi r^3 + \kappa c^2 m(r)) (\rho c^2 + P(r))}{2r (\kappa c^2 m(r) + \frac{4}{3} r \pi (\Lambda r^2 - 3))} \\
& - \alpha^2 \frac{72 (\rho c^2 + P(r))}{r (4 \Lambda \pi r^3 + 3 \kappa c^2 m(r) - 12 r \pi)^2} \\
& \times \left\{ \frac{\pi r}{3} \ln\left(\frac{b^2}{r^2}\right) \left[\frac{3}{4} \kappa c^2 (\Lambda r^2 + 1) m(r) \right. \right. \\
& + \pi [\kappa (\Lambda r^2 + 3) P(r) - 4 \Lambda] r^3 \left. \right] + \frac{1}{4} \kappa^2 (m(r))^2 c^4 \\
& + \pi c^2 \kappa m(r) r \left[\kappa P(r) \ln(r) r^2 + (-\Lambda r^2 + 1) \ln(r) \right. \\
& + \frac{2}{3} \Lambda r^2 - \frac{7}{4} \left. \right] + \pi^2 r \left[r^2 \kappa P(r) (\kappa c^2 N(r) + \frac{2}{3} \Lambda r^3 \right. \\
& - r) - \kappa c^2 N(r) (\Lambda r^2 - 1) - \frac{2}{9} r^5 \Lambda^2 \\
& \left. \left. - \frac{2}{3} \Lambda r^3 + 2r \right] \right\}, \tag{16}
\end{aligned}$$

in which $N(r) = \int -4r^2 \ln(r) \rho(r) dr$. As can be seen, the first term on the right-hand side of this equation is the well-known TOV equation, and the second term is considered as a correction term in dilaton gravity. On close inspection of Equation (16), in the case of $\alpha = 0$, the new HEE equation will be exactly the same as TOV.

4 STRUCTURE OF STRANGE QUARK STARS IN DILATON GRAVITY

In this section, we calculate some structural properties of SQSs in dilaton gravity. To obtain the configurational characteristics of the quark stars, we must solve the HEE equation, Equation (16), numerically by using an EoS in the form $P = P(\rho)$.

4.1 EoS of Strange Quark Matter

We obtain the EoS of SQM using the MIT bag model. In this model, the total energy is the sum of kinetic energy of quarks plus a bag constant (B_{bag}) (Chodos et al. 1974). In fact, the bag constant B_{bag} can be interpreted as the difference between the energy densities of noninteracting quarks and interacting ones. Dynamically it acts as a pressure, which keeps the quark gas at constant density and potential. The value of bag constant, B_{bag} , lies in the interval $58.8 \text{ MeV fm}^{-3} < B_{\text{bag}} < 91.2 \text{ MeV fm}^{-3}$ (Stergioulas 2003) and in this work, the values 60, 75 and 90 MeV fm^{-3} are considered for the bag constant. In order to obtain the EoS, we have neglected the mass of u and d quarks and

considered the mass of an s quark to be $m_s = 150 \text{ MeV}$. More details on the EoS of SQM can be found in Bordbar & Peivand (2011).

In Figure 1, we plot the behavior of the EoS for SQM in the MIT bag model for various values of B_{bag} . This figure demonstrates that for all values of bag constant, the EoS of SQM can be treated as linear. Also, it is observed that an EoS for SQM with a lower value of B_{bag} is stiffer than the higher case. In the next section, we calculate maximum mass and corresponding radius of an SQS in dilaton gravity by using this EoS and Equation (16) (also Eq. (15)).

4.2 Maximum Mass of an SQS in Dilaton Gravity

Like other compact objects, SQSs reach a limiting gravitational mass known as the maximum mass. Subsequently, we can obtain the maximum mass (M_{max}) of an SQS in dilaton gravity in the states with various values of α and Λ , by numerically integrating Equation (16) (or Eq. (15)) and using the EoS of SQM.

In Table 1, we calculate and present the structural properties of an SQS with varying α with the reported value of cosmological constant ($\Lambda \leq 10^{-56} \text{ cm}^{-2}$) and for a vanishing cosmological constant. As we can see, these values of Λ and α do not have a significant impact on the structural properties of an SQS.

Finding the exact value of the cosmological constant is an open issue. Although its reported value can be valid in large-scale structure, when we encounter a local scale structure close to a massive object, such as a neutron star or SQS, the value of Λ may be very different from its reported value for large-scale structure (Bordbar et al. 2016). Motivated by this reason, $\Lambda \leq 10^{-13} \text{ cm}^{-2}$ has been applied to investigate the structural properties of compact objects in the presence of cosmological constant by several authors (Hendi et al. 2015; Bordbar et al. 2016; Zubairi et al. 2015). In addition, it is notable that some cosmological models consider Λ as a decreasing variable with time, which has been predicted by decaying vacuum energy (Waga 1993; Böhmer & Harko 2005b). Therefore, considering the effect of such differing values of the cosmological constant on structural properties of a compact object can be interesting. In the remainder of this section, we have used $\Lambda \leq 10^{-13} \text{ cm}^{-2}$ to examine the bulk properties of SQSs in dilaton gravity.

In Figure 2, we plot the gravitational mass-radius for $\Lambda = \alpha = 0$. The values of maximum mass and corresponding values of radius are listed in Table 2. As is apparent, these values are the same as M_{max} and R in Einstein gravity (Bordbar & Peivand 2011).

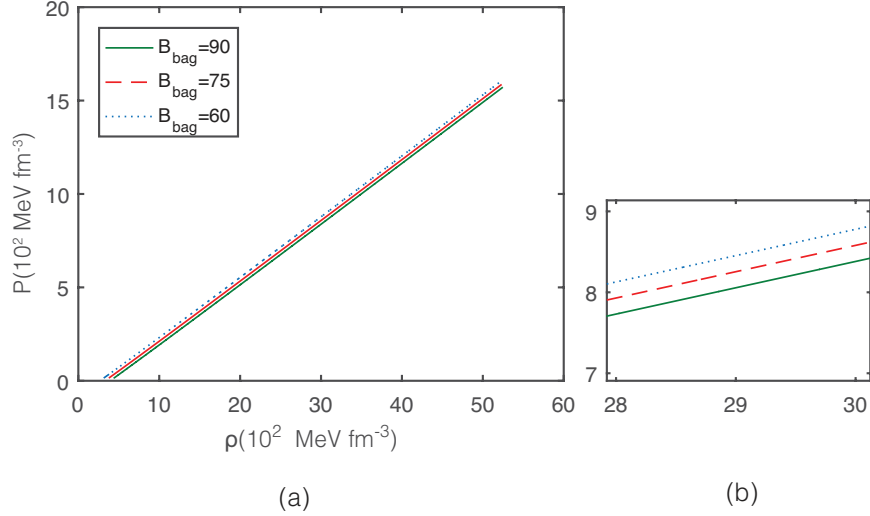


Fig. 1 EoS of SQM for various values of bag constant (*left panel*). The right panel features an enlarged view of the left one.

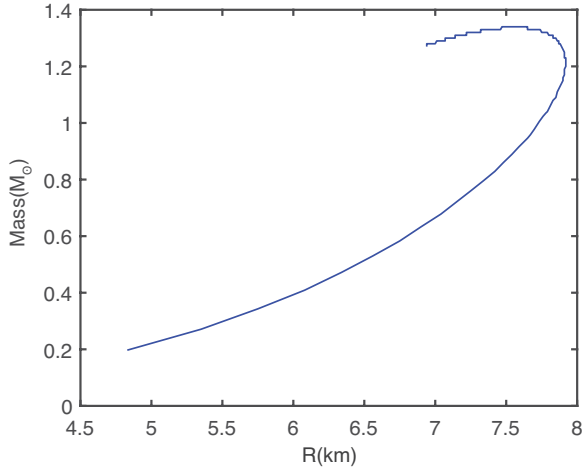


Fig. 2 The mass-radius relation of an SQS for $\Lambda = 0$ ($\alpha = 0$, $b = 10^{-4}$ and $B_{\text{bag}} = 90 \text{ MeV fm}^{-3}$).

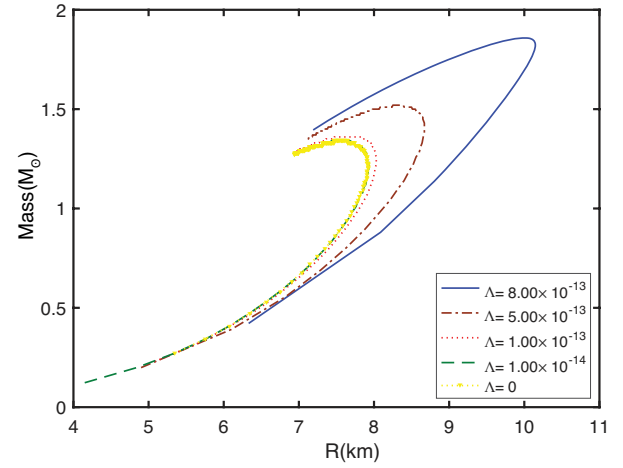


Fig. 3 The mass-radius relation of an SQS for various positive values of Λ ($\alpha = 0$, $b = 10^{-4}$ and $B_{\text{bag}} = 90 \text{ MeV fm}^{-3}$).

The gravitational mass versus radius and central energy density for a constant value of α but different values of Λ is plotted in Figures 3 and 5, respectively. We have also plotted the effective gravitational mass versus effective radius (see Fig. 4). Figure 3 demonstrates that an increase in Λ has led to an increase in the maximum mass. Moreover, for $\Lambda \leq 10^{-14}$ deviation of the $M - R$ relation from Einstein gravity is very small (see Fig. 3). This result is repeated in Figure 4 and it can be ascertained that values of the gravitational mass and corresponding radius are the same as effective mass and corresponding effective radius respectively (see Table 2). For a given central energy density (ρ_c), the mass of SQS increases by increasing cosmological constant (see Fig. 5). We can find that for higher values of the cosmological constant, gravitational mass in-

creases at a higher rate and reaches M_{max} in SQSs with smaller values of central energy density (ρ_c).

In Figure 6, we investigate the quark star structure for a given positive value of Λ but for different values of α , which demonstrates that variations in dilaton parameter α do not affect the SQS structure. It should be noted that there is no answer to the dilaton HEE for $\alpha \geq 10^{-4}$. $B_{\text{bag}} = 90 \text{ MeV fm}^{-3}$ is considered in the figures drawn so far. In Figure 7, we plot the mass-radius relation of an SQS in dilaton gravity for $B_{\text{bag}} = 60$ and 75 MeV fm^{-3} for a given value of Λ and different values of α . It can be seen that in these situations, the lack of influence of α on the mass and radius of SQS still remains. Values of the maximum mass and corresponding radius values in these modes are shown in Tables 3 and 4.

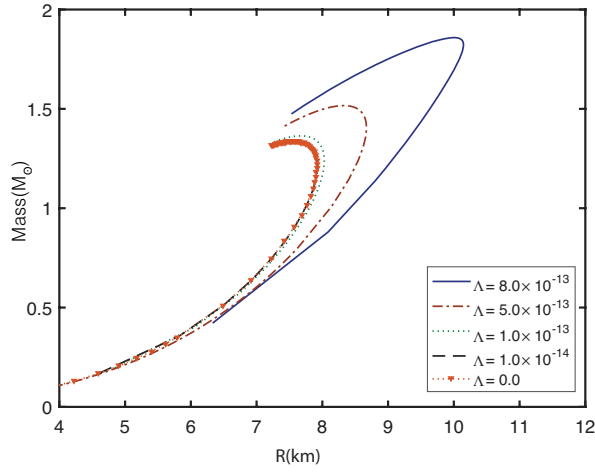


Fig. 4 The effective mass-effective radius relation of an SQS for various positive values of Λ ($\alpha = 0$, $b = 10^{-4}$ and $B_{\text{bag}} = 90 \text{ MeV fm}^{-3}$).

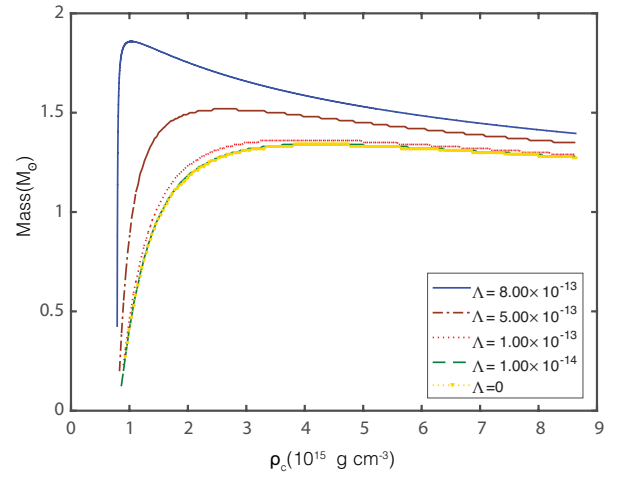


Fig. 5 The gravitational mass versus total central energy density of an SQS with various values of Λ at $\alpha = 0$, $b = 10^{-4}$ and $B_{\text{bag}} = 90 \text{ MeV fm}^{-3}$.

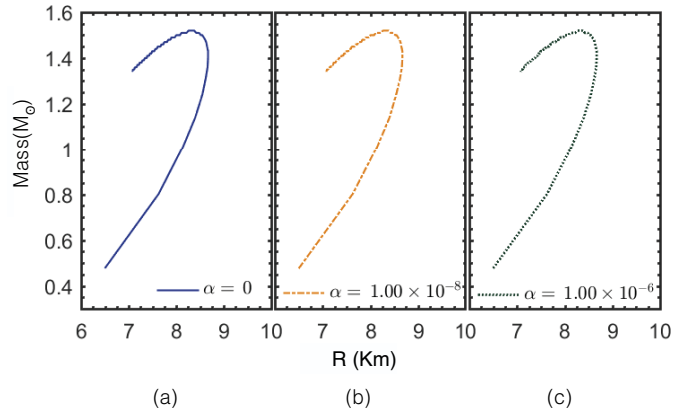


Fig. 6 The mass-radius relation of an SQS for $\Lambda = 5.00 \times 10^{-13}$ at (a) $\alpha = 0$, (b) $\alpha = 1.00 \times 10^{-8}$ and (c) $\alpha = 1.00 \times 10^{-6}$.

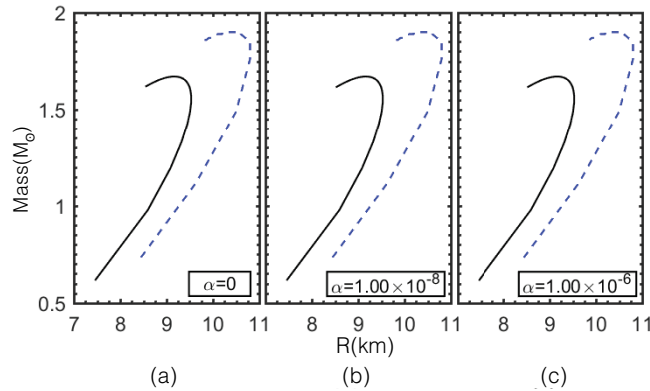


Fig. 7 Same as Fig. 6, but for $B_{\text{bag}} = 60 \text{ MeV fm}^{-3}$ (dashed lines) and $B_{\text{bag}} = 75 \text{ MeV fm}^{-3}$ (solid lines).

In Figure 8, the maximum gravitational mass as a function of Λ in all cases of B_{bag} is plotted. This indicates that M_{max} is an increasing function of Λ . However, the rate of increase for M_{max} versus Λ increases with an increasing bag constant.

In Figure 9, we plot the energy per baryon (E/A) for SQM with the various values of bag constant as a function of pressure. We see that the zero point of pressure for SQM considered with lower values of B_{bag} has a lower E/A .

Table 1 Maximum gravitational mass (M_{\max}) and the corresponding radius (R) of an SQS in dilaton gravity for various positive values of Λ and α with various values of B_{bag} .

B_{bag} (MeV fm $^{-3}$)	α	Λ	M_{\max} (M_{\odot})	R (km)	$\bar{\rho}$ (10^{15} g cm $^{-3}$)	z (10^{-1})
60	0	0	1.55	8.86	1.06	4.37
	1.00×10^{-8}	0	1.55	8.86	1.06	4.37
	1.00×10^{-5}	0	1.55	8.86	1.06	4.37
	0	1.00×10^{-56}	1.55	8.86	1.06	4.37
	1.00×10^{-8}	1.00×10^{-56}	1.55	8.86	1.06	4.37
	1.00×10^{-5}	1.00×10^{-56}	1.55	8.86	1.06	4.37
75	0	0	1.43	8.15	1.25	4.40
	1.00×10^{-8}	0	1.43	8.15	1.25	4.40
	1.00×10^{-5}	0	1.43	8.15	1.25	4.40
	0	1.00×10^{-56}	1.43	8.15	1.25	4.40
	1.00×10^{-8}	1.00×10^{-56}	1.43	8.15	1.25	4.40
	1.00×10^{-5}	1.00×10^{-56}	1.43	8.15	1.25	4.40
90	0	0	1.34	7.58	1.46	4.45
	1.00×10^{-8}	0	1.34	7.58	1.46	4.45
	1.00×10^{-5}	0	1.34	7.58	1.46	4.45
	0	1.00×10^{-56}	1.34	7.58	1.46	4.45
	1.00×10^{-8}	1.00×10^{-56}	1.34	7.58	1.46	4.45
	1.00×10^{-5}	1.00×10^{-56}	1.34	7.58	1.46	4.45

Table 2 Maximum gravitational mass (M_{\max}) and the corresponding radius (R) of an SQS in dilaton gravity for various positive values of Λ at $b = 10^{-4}$ and $\alpha = 0$.

Λ	M_{\max} (M_{\odot})	R (km)	M_{\max}^{eff} (M_{\odot})	R^{eff} (km)	$\bar{\rho}$ (10^{15} g cm $^{-3}$)	z_{eff} (10^{-1})	z (10^{-1})
0	1.34	7.58	1.34	7.58	1.46	4.45	4.45
1.00×10^{-14}	1.34	7.58	1.34	7.58	1.43	4.48	4.48
1.00×10^{-13}	1.36	7.68	1.36	7.68	1.43	4.78	4.78
3.00×10^{-13}	1.43	7.95	1.43	7.95	1.35	5.69	5.69
4.00×10^{-13}	1.47	8.13	1.47	8.13	1.30	6.25	6.25
5.00×10^{-13}	1.52	8.34	1.52	8.34	1.24	6.99	6.99
8.00×10^{-13}	1.86	10.01	1.86	10.01	0.88	13.27	13.27

Table 3 Maximum gravitational mass (M_{\max}) and the corresponding radius (R) of an SQS in dilaton gravity for various positive values of Λ and α with $B_{\text{bag}} = 60$ MeV fm $^{-3}$.

α	Λ	M_{\max} (M_{\odot})	R (km)	$\bar{\rho}$ (10^{15} g cm $^{-3}$)	z (10^{-1})	B_{bag} (MeV fm $^{-3}$)
1.00×10^{-7}	1.00×10^{-15}	1.55	8.86	1.06	4.38	60
1.00×10^{-7}	1.00×10^{-14}	1.55	8.88	1.06	4.41	60
0	1.00×10^{-13}	1.59	9.04	1.02	4.84	60
0	3.00×10^{-13}	1.71	9.53	0.94	6.22	60
0	4.00×10^{-13}	1.78	9.87	0.88	7.20	60
0	5.00×10^{-13}	1.90	10.43	0.80	8.85	60
1.00×10^{-8}	5.00×10^{-13}	1.90	10.43	0.80	8.85	60
1.00×10^{-6}	5.00×10^{-13}	1.90	10.43	0.80	8.85	60

This implies that some SQM modeled with lower values of B_{bag} is more stable than others.

In Table 5, we give the percentage increase of maximum mass of an SQS and we apply various values of the bag constant to calculate EoS of SQM in different values of Λ with respect to obtained M_{\max} in GR ($\alpha = \Lambda = 0$) with the same value of B_{bag} (for instance $(\Delta M)_{\Lambda_1}^{B=90} = (M_{\max})_{\Lambda_1=1 \times 10^{-13}}^{B=90} - (M_{\max})_{\Lambda_0=0}^{B=90} = 0.02 M_{\odot} = 1.49\% (M_{\max})_{\Lambda_0=0}^{B=90}$ derived for $B_{\text{bag}} = 90$).

We can see that the effect of Λ on SQSs that have higher stability is larger than the other ones (see columns in Table 5). In addition, this table shows that the increasing rate of the percentage increase of maximum mass for an SQS, is enhanced by enhancing Λ (see rows in Table 5).

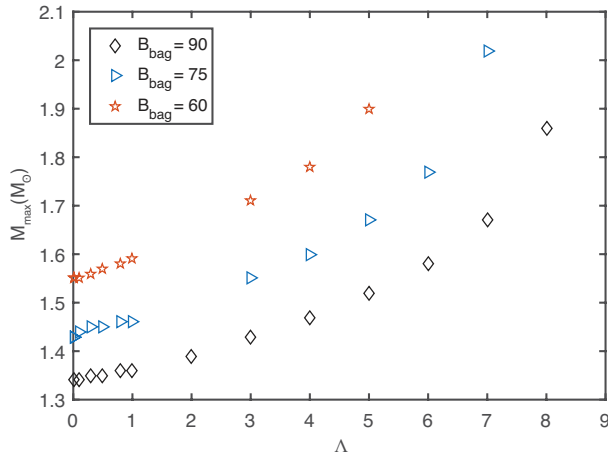
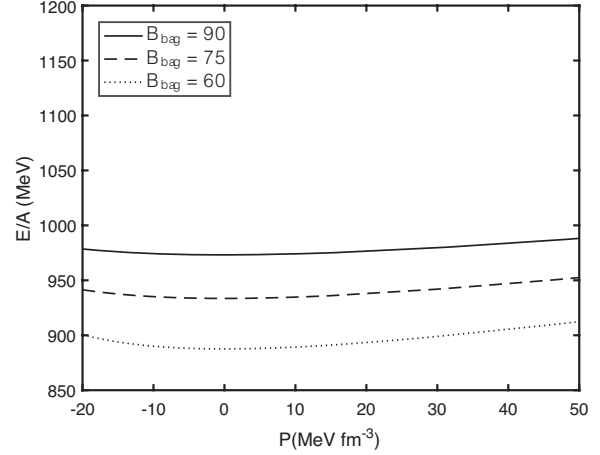
Negative values of Λ are investigated in Figure 10 with a particular value of α to obtain the SQS structure. As we can see, increasing the maximum mass and its correspond-

Table 4 Maximum gravitational mass (M_{\max}) and the corresponding radius (R) of an SQS in dilaton gravity for various positive values of Λ and α with $B_{\text{bag}} = 75 \text{ MeV fm}^{-3}$.

α	Λ	$M_{\max} (M_{\odot})$	R (km)	$\bar{\rho} (10^{15} \text{ g cm}^{-3})$	$z (10^{-1})$	$B_{\text{bag}} (\text{MeV fm}^{-3})$
1.00×10^{-7}	1.00×10^{-15}	1.43	8.15	1.25	4.40	75
1.00×10^{-7}	1.00×10^{-14}	1.44	8.15	1.26	4.48	75
1.00×10^{-8}	1.00×10^{-13}	1.46	8.30	1.21	4.77	75
0	1.00×10^{-13}	1.46	8.30	1.21	4.77	75
0	3.00×10^{-13}	1.55	8.63	1.15	5.90	75
0	4.00×10^{-13}	1.60	8.87	1.09	6.60	75
0	5.00×10^{-13}	1.67	9.18	1.03	7.60	75
1.00×10^{-8}	5.00×10^{-13}	1.67	9.18	1.03	7.60	75
1.00×10^{-6}	5.00×10^{-13}	1.67	9.18	1.03	7.60	75

Table 5 The percentage increase of maximum mass of an SQS in dilaton gravity for various values of Λ at $b = 10^{-4}$ and $\alpha = 0$ with different values of B_{bag} .

B_{bag}	$(\Delta M)_{\Lambda_1} [M_{\max \Lambda_1}]$ ($\Lambda_1 = 1.00 \times 10^{-13}$)	$(\Delta M)_{\Lambda_2} [M_{\max \Lambda_2}]$ ($\Lambda_2 = 3.00 \times 10^{-13}$)	$(\Delta M)_{\Lambda_3} [M_{\max \Lambda_3}]$ ($\Lambda_3 = 4.00 \times 10^{-13}$)	$(\Delta M)_{\Lambda_4} [M_{\max \Lambda_4}]$ ($\Lambda_4 = 5.00 \times 10^{-13}$)
90	1.49%	6.72%	9.70%	13.43%
75	2.10%	8.39%	11.89%	16.78%
60	2.58%	10.32%	14.84%	22.58%

**Fig. 8** Maximum mass of an SQS versus cosmological constant ($\times 10^{-13}$) for different bag constants with $\alpha = 0$.**Fig. 9** The energy per baryon versus the pressure (P) for SQSs with the various values of bag constant.

ing radius is simultaneous with increasing cosmological constant using negative values (also see Table 6).

Table 6 Maximum gravitational mass (M_{\max}) and the corresponding radius (R) of SQS in dilaton gravity for various negative values of Λ at $b = 10^{-4}$ and $\alpha = 0$.

α	Λ	$M_{\max} (M_{\odot})$	R (km)
0	0	1.34	7.57
0	-8.00×10^{-13}	1.19	6.94
0	-1.00×10^{-12}	1.16	6.83

It should be noted that for $\Lambda \geq 10^{-12}$, HEE in dilaton gravity does not have a logical answer. The structural results for $\Lambda < 10^{-14}$ are similar to those for $\Lambda = 0$.

4.3 Redshift and Mean Density

Information about the compactness of a compact object, mass-radius ratio, can be found from the gravitational redshift, which is an observational quantity (denoted by z). We can obtain z by using Equation (14) in two forms:

$$z_{\text{eff}} = \left\{ \left[-\frac{\Lambda (\Upsilon)^{\alpha^2}}{3K_{1,-1}} - \frac{\Upsilon \alpha^2}{K_{1,-1}^2 b^2} + \frac{(\Upsilon)^{-\alpha^2}}{\Omega^2 K_{1,-1}} \right] \Omega^2 K_{1,1}^2 - \frac{2G K_{1,1} M_{\text{eff}} \Omega^{-\frac{K_{1,-3}}{K_{1,1}}}}{c^2} \right\}^{-\frac{1}{2}} - 1, \quad (17)$$

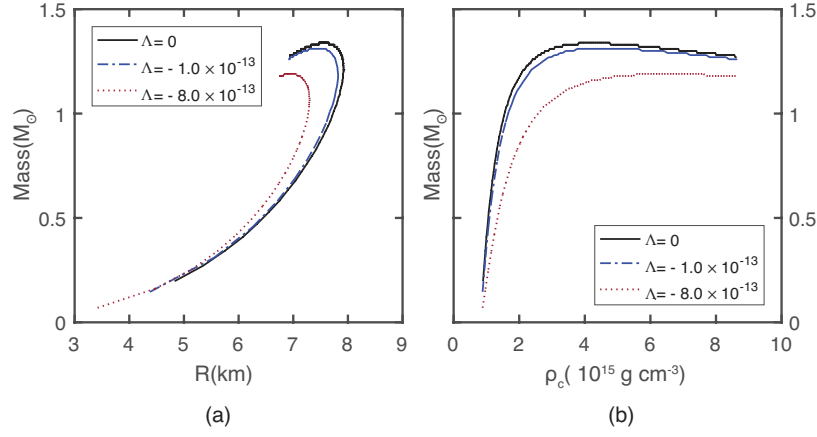


Fig. 10 The gravitational mass versus (a) corresponding radius and (b) central energy density (ρ_c) of an SQS in dilaton gravity for negative values of Λ ($\alpha = 0$, $b = 10^{-4}$ and $B_{\text{bag}} = 90 \text{ MeV fm}^{-3}$).

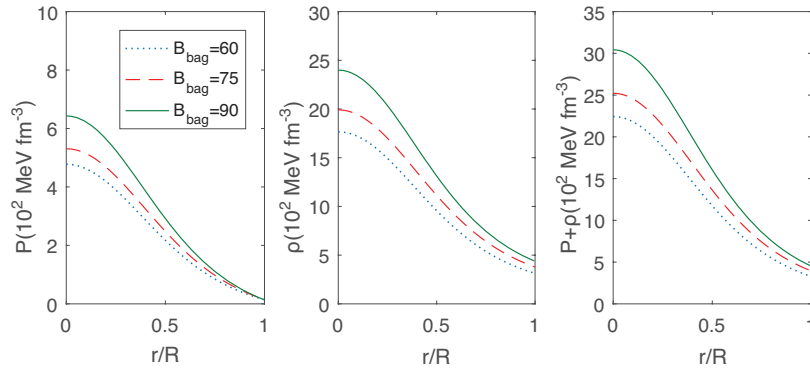


Fig. 11 The behavior of pressure P , energy density ρ and $P + \rho$ with respect to fractional radius $\frac{r}{R}$ under various values of B_{bag} with $\alpha = \Lambda = 0$.

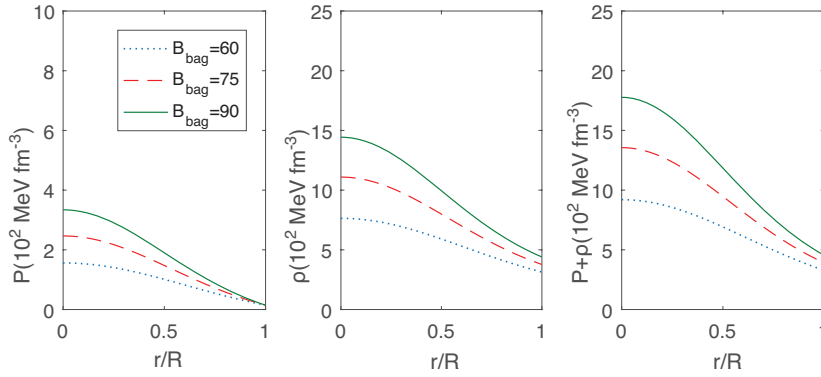


Fig. 12 Same as Fig. 11 for $\alpha = 1 \times 10^{-6}$ and $\Lambda = 5 \times 10^{-13}$.

and

$$\begin{aligned}
 z = & \left\{ \left[1 - \frac{2GM}{Rc^2} - \frac{\Lambda R^2}{3} \right] \right. \\
 & + \frac{\alpha^2}{3Rc^2} \left[-Rc^2(R^2\Lambda + 3) \ln\left(\frac{b^2}{R^2}\right) \right. \\
 & \left. \left. + (-3\Lambda R^3 + 6R)c^2 - 14GM \right] \right\}^{-\frac{1}{2}} - 1, \quad (18)
 \end{aligned}$$

where in Equation (17), $\Omega = \sigma\delta$ and Υ are functions of R_{eff} and to obtain Equation (18), we have expanded Equation (14) in a series of α and neglected all terms of order higher than 2.

In Tables 2 to 4 we have evaluated z and $\bar{\rho} = \frac{3M}{4\pi R^3}$ (the mean energy density) for an SQS in different cases. For all cases, we can see that with increasing Λ , gravita-

tional redshift increases while $\bar{\rho}$ decreases (see Table 2 and Table 4). We can ascertain that increasing Λ is equivalent to increasing B_{bag} . Therefore, it can be interpreted as increasing the values of the difference between the energy densities of non-interacting quarks and interacting quarks. In addition, we can find that for fixed values of Λ , variations of α do not affect z or $\bar{\rho}$.

4.4 Energy Conditions

Any acceptable physical model of isotropic fluid must satisfy conditions on energy (Hendi et al. 2016a; Visser & Barcelo 2000). The variations of pressure and energy density of an SQS with respect to fractional radius are shown in Figure 11 and 12. As we can see, the pressure of the system is non-zero and positive at the origin. In addition, it is clear that the pressure and energy density decrease monotonically by increasing fractional radius. Moreover, it is observed that pressure reaches zero at the boundary of the star ($r = R$) in all cases. In addition, the sum of pressure and energy density versus $\frac{r}{R}$ throughout the star is also shown in these figures. It is clear that all energy conditions for a perfect fluid are satisfied for an SQS in dilaton gravity.

4.5 Matching Interior and Exterior Solutions

In this part, we investigate interior and exterior solutions at the matching boundaries by noting that we have assumed $\rho = \bar{\rho}$ throughout the star. At first, we can find the interior radial component of metric tensor ($\frac{1}{A(r)}$) by expanding Equation (14) in a series of α and neglecting all terms of order higher than 2, therefore for $r < R$ we have

$$\begin{aligned} A(r)_{\text{in}} = & \left[1 - \frac{\Lambda r^2}{3} - \frac{\kappa c^2 m(r)}{4\pi r} \right] \\ & + \left[2 - \frac{1}{3} \Lambda r^2 \ln\left(\frac{b^2}{r^2}\right) - \Lambda r^2 - \ln\left(\frac{b^2}{r^2}\right) \right. \\ & - \frac{\kappa c^2 m(r)}{4\pi r} + \frac{4}{3} \kappa \bar{\rho} c^2 r^2 \ln(r) - \frac{4}{9} \kappa \bar{\rho} c^2 r^2 \\ & \left. - \frac{\kappa c^2 m(r) \ln(r)}{\pi r} \right] \alpha^2, \end{aligned} \quad (19)$$

which by replacing $m(r) = \frac{M}{R^3} r^3$ and $\bar{\rho} = \frac{3M}{4\pi R^3}$ yields

$$\begin{aligned} A(r)_{\text{in}} = & \left[1 - \frac{\Lambda r^2}{3} - \frac{\kappa c^2 M}{4\pi R^3} r^2 \right] \\ & + \left[2 - \frac{1}{3} \Lambda r^2 \ln\left(\frac{b^2}{r^2}\right) - \Lambda r^2 \right. \\ & \left. - \ln\left(\frac{b^2}{r^2}\right) - \frac{7\kappa c^2 M}{12\pi R^3} r^2 \right] \alpha^2. \end{aligned} \quad (20)$$

We can calculate time component ($B(r)$) of internal metric tensor by integrating Equation (13) from a specific value of r ($r < R$) to the surface of the star ($r = R$). We obtain

$$B(r)_{\text{in}} = B(R) \left(\frac{\bar{\rho} c^2}{P(r) + \bar{\rho} c^2} \right)^2, \quad (21)$$

where $B(R)$ is the time component of metric at the surface and $P(r)$ is pressure at a specified radius that can be determined by numerically integrating Equation (16). It is notable that if one inserts $r = R$ in Equation (21) ($P(r = R) = 0$), then $B(r)_{\text{in}} = B(R)$.

We can derive exterior radial and time components of the metric by solving Equations (10) and (11) and also considering that outside of the star, $P(r) = \rho(r) = 0$. Then, for $r > R$, we have

$$\begin{aligned} A(r)_{\text{out}} = B(r)_{\text{out}} = & \left[1 - \frac{\Lambda r^2}{3} - \frac{\kappa c^2 M}{4\pi r} \right] \\ & + \left[2 - \frac{\Lambda r^2 \ln\left(\frac{b^2}{r^2}\right)}{3} - \Lambda r^2 - \ln\left(\frac{b^2}{r^2}\right) \right. \\ & \left. - \frac{7\kappa c^2 M}{12\pi r} + \frac{\kappa c^2 M}{\pi r} \ln\left(\frac{R}{r}\right) \right] \alpha^2. \end{aligned} \quad (22)$$

According to Equations (19)–(22), we can easily see that the interior solution smoothly matches the exterior solution at the surface of the star ($r = R$).

In Figures 13 and 14, we have plotted $\frac{1}{A(r)}$ and $B(r)$ against fractional radius ($\frac{r}{R}$) for different values of α , Λ and B_{bag} . We can see that the components of the metric at the center of the object are non-singular and positive (Shee et al. 2018). Also, these figures demonstrate that $\frac{1}{A(r)}$ and $B(r)$ are a monotonically increasing functions of $\frac{r}{R}$ throughout the star as proved by Lake (2003) for any physically acceptable model.

5 STABILITY

5.1 Speed of Sound

When we examine the stability of a compact object in terms of the speed of sound, two conditions must be satisfied

- (1) *The causality condition:* Speed of sound (v_s) has to be positive and less than the speed of light (c). The variations of $\frac{v_s^2}{c^2}$ with the fractional radius and energy density ($\frac{\rho}{\rho_c}$) are shown in Figure 15 and 16. It is observed that the speed of sound lies between 0 and 1 inside the quark star in all cases. Also, v_s decreases with increasing (decreasing) radius (energy density) of the star and reaches its minimum value at the surface.

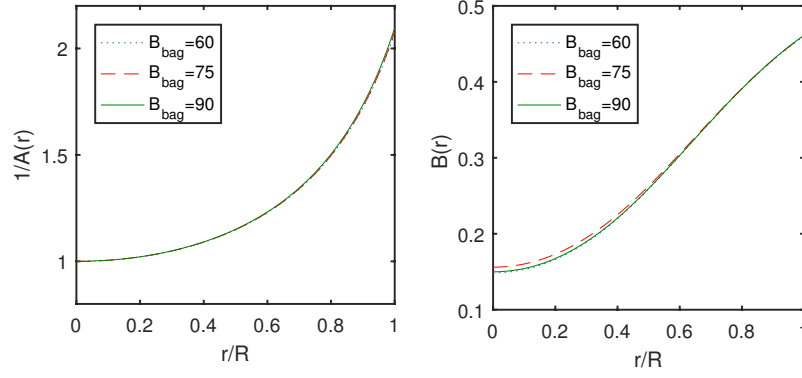


Fig. 13 The variations in radial and time components of metric tensor with respect to fractional radius $\frac{r}{R}$ under various values of B_{bag} with $\alpha = \Lambda = 0$.

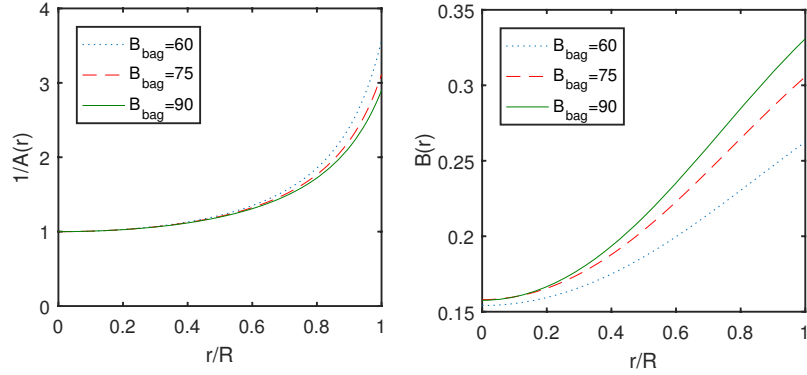


Fig. 14 Same as Fig. 13 but for $\alpha = 1 \times 10^{-6}$ and $\Lambda = 5 \times 10^{-13}$.

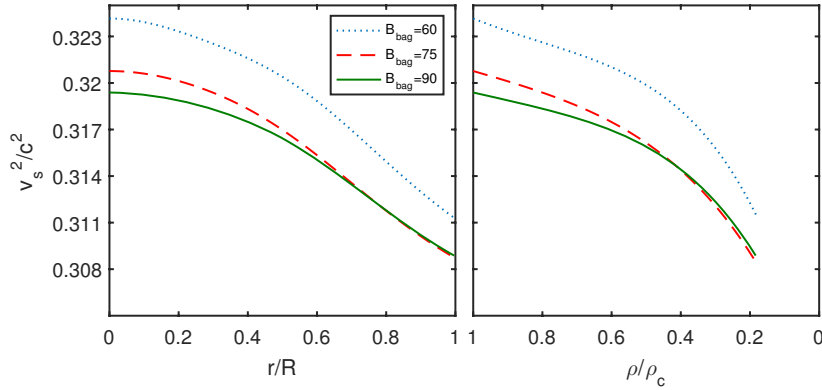


Fig. 15 The behavior of $\frac{v_s^2}{c^2}$ with respect to fractional radius $\frac{r}{R}$ (left panel) and fractional energy density $\frac{\rho}{\rho_c}$ (right panel) under various values of B_{bag} with $\alpha = \Lambda = 0$.

(2) *Herrera cracking*: The concept of cracking proposed by Herrera (1992) has been applied to investigating the stability of an *anisotropic* compact object (Shee et al. 2018; Deb et al. 2017; Maurya et al. 2018). We do not need to check for cracking, because the model that we considered here is an isotropic quark star and the pressure of the star is equal in all directions (see Eq. (9)).

5.2 Adiabatic Index

An essential criterion for the dynamical stability of a compact object against radial adiabatic infinitesimal perturbations is determined by the adiabatic index Γ

$$\Gamma = \frac{\rho}{P} \left(1 + \frac{P}{\rho c^2} \right) \frac{dP}{d\rho}. \quad (23)$$

Chandrasekhar showed that for the dynamical stability of a compact object, Γ must be greater than $\frac{4}{3}$ throughout

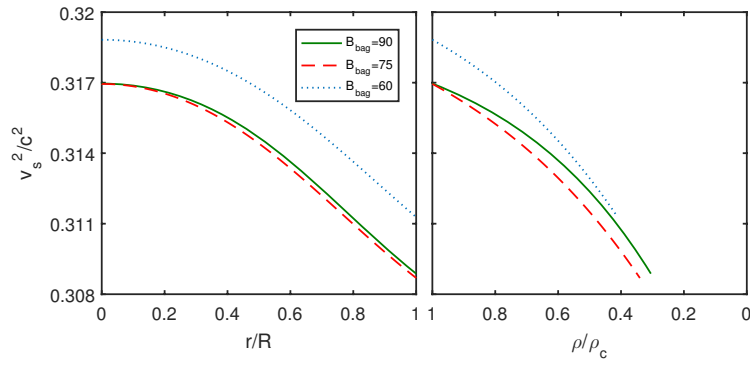


Fig. 16 Same as Fig. 15 but for $\alpha = 1 \times 10^{-6}$ and $\Lambda = 5 \times 10^{-13}$.

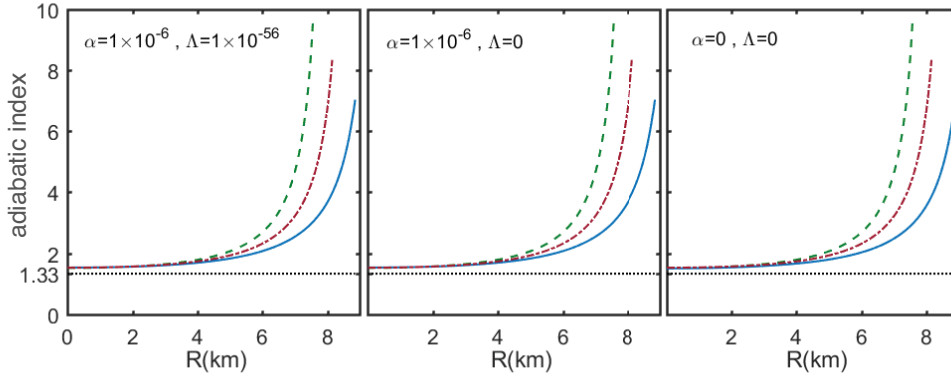


Fig. 17 The variation in adiabatic index with radial coordinate r for different cases of α and Λ with $B_{\text{bag}} = 60 \text{ MeV fm}^{-3}$ (solid line), $B_{\text{bag}} = 75 \text{ MeV fm}^{-3}$ (dash-dotted line) and $B_{\text{bag}} = 90 \text{ MeV fm}^{-3}$ (dashed line).

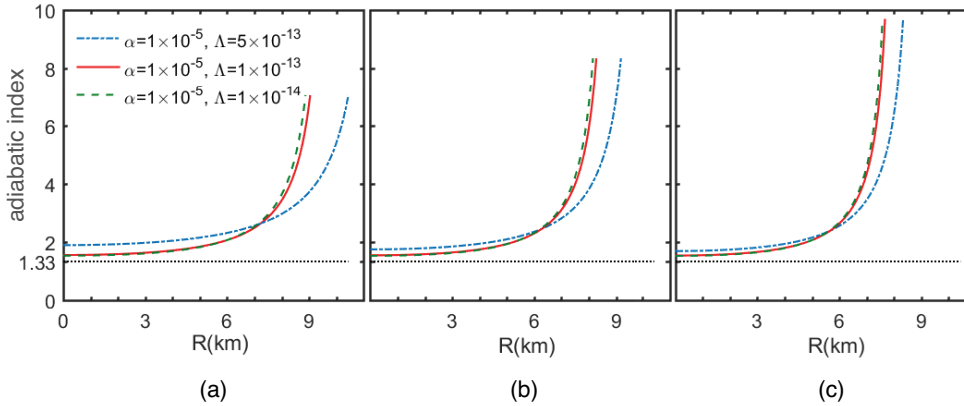


Fig. 18 The variation in adiabatic index with radial coordinate r under various conditions of α and Λ in (a) $B_{\text{bag}} = 60 \text{ MeV fm}^{-3}$, (b) $B_{\text{bag}} = 75 \text{ MeV fm}^{-3}$ and (c) $B_{\text{bag}} = 90 \text{ MeV fm}^{-3}$.

it (Chandrasekhar 1964). The variation of Γ versus radial coordinate r is shown in Figures 17 and 18 for different cases of α , Λ and bag constant. One can see that the variation of α has no effect on the adiabatic index values, while the variation of Λ increases the rate of increase in Γ . In amounts other than the reported value of Λ , the adiabatic index reaches greater values near the surface of the star with larger values of bag constant (see Fig. 18). We can

also see in Figures 17 and 18 that the values of Γ for the central layers of an SQS star are closer to and greater than $\frac{4}{3}$ but for layers near the surface they are very large. In all of the cases that we have considered here, the values of Γ are higher than $\frac{4}{3}$.

Therefore, we can conclude that an SQS in dilaton gravity is stable with all values of bag constant that we have considered due to the causality condition and because

the adiabatic index inequality ($\Gamma \geq \frac{4}{3}$) is valid everywhere inside the star.

6 CONCLUSIONS

We obtained the HEE of a compact object in dilaton gravity by using two approaches. Then, by employing the obtained HEEs we calculated some structural properties of an SQS. We assumed that the dilaton gravity has been constructed from a dilaton field with a potential, including two Liouville type terms in the context of Einstein gravity. We found that with the values of α and Λ where HEE in dilaton gravity has a logical answer, the SQS does not change with variations in α . This behavior also persists with different values of the bag constant. On the other hand, increasing Λ enhances the maximum mass. We ascertain that the percentage increase of maximum mass for an SQS has higher values for SQSs that are more stable than others. We demonstrate that the effect of dilaton gravity and applying smaller bag constant in the EoS of SQM on the SQS leads to SQSs with bigger masses and radii which are more stable than SQSs in Einstein gravity. We also show that SQSs in dilaton gravity are stable against radial adiabatic infinitesimal perturbations in all of the cases that we considered here. Moreover, our results indicate that the causality condition and energy conditions are valid for the model that we considered. Since the values of M_{\max} and radius for $\Lambda < 10^{-14}$ are the same values for $\Lambda = 0$, and cosmological observations suggest $\Lambda \leq 3 \times 10^{-56} \text{ cm}^{-2}$, it can be concluded that this limit on the cosmological constant does not affect the structure of an SQS in dilaton gravity.

Acknowledgements G. H. Bordbar wishes to thank the Shiraz University Research Council. This work has been supported by the Research Institute for Astronomy and Astrophysics of Maragha.

References

- Alcock, C., Farhi, E., & Olinto, A. 1986a, *Physical Review Letters*, 57, 2088
- Alcock, C., Farhi, E., & Olinto, A. 1986b, *ApJ*, 310, 261
- Alcock, C., & Olinto, A. 1988, *Annual Review of Nuclear and Particle Science*, 38, 161
- Arapoğlu, S., Deliduman, C., & Ekşi, K. Y. 2011, *J. Cosmol. Astropart. Phys.*, 7, 020
- Astashenok, A. V., Capozziello, S., & Odintsov, S. D. 2013, *J. Cosmol. Astropart. Phys.*, 12, 040
- Astashenok, A. V., Capozziello, S., & Odintsov, S. D. 2015, *Physics Letters B*, 742, 160
- Astashenok, A. 2016, in *International Journal of Modern Physics: Conference Series*, 41 (World Scientific), 1660130
- Balaguera-Antolínez, A., Nowakowski, M., & Böhmer, C. G. 2005, *International Journal of Modern Physics D*, 14, 1507
- Böhmer, C. G., & Harko, T. 2005a, *Physics Letters B*, 630, 73
- Böhmer, C. G., & Harko, T. 2005b, *Phys. Rev. D*, 71, 084026
- Bombaci, I. 1997, *Phys. Rev. C*, 55, 1587
- Bordbar, G. H., Bigdeli, M., & Yazdizadeh, T. 2006, *International Journal of Modern Physics A*, 21, 5991
- Bordbar, G. H., Hendi, S. H., & Eslam Panah, B. 2016, *European Physical Journal Plus*, 131, 315
- Bordbar, G. H., & Peivand, A. R. 2011, *RAA (Research in Astronomy and Astrophysics)*, 11, 851
- Chan, K. C. K., Horne, J. H., & Mann, R. B. 1995, *Nuclear Physics B*, 447, 441
- Chandrasekhar, S. 1964, *Physical Review Letters*, 12, 114
- Cho, Y. M. 1990, *Phys. Rev. D*, 41, 2462
- Chodos, A., Jaffe, R. L., Johnson, K., Thorn, C. B., & Weisskopf, V. F. 1974, *Phys. Rev. D*, 9, 3471
- Deb, D., Chowdhury, S. R., Ray, S., Rahaman, F., & Guha, B. K. 2017, *Annals of Physics*, 387, 239
- Dehghani, M. H., & Farhangkhan, N. 2005, *Phys. Rev. D*, 71, 044008
- Demorest, P. B., Pennucci, T., Ransom, S. M., Roberts, M. S. E., & Hessels, J. W. T. 2010, *Nature*, 467, 1081
- Dey, M., Bombaci, I., Dey, J., Ray, S., & Samanta, B. C. 1998, *Physics Letters B*, 438, 123
- Farhi, E., & Jaffe, R. L. 1984, *Phys. Rev. D*, 30, 2379
- Gangopadhyay, T., Ray, S., Li, X.-D., Dey, J., & Dey, M. 2013, *MNRAS*, 431, 3216
- Glendenning, N. K. 1990, *Modern Physics Letters A*, 5, 2197
- Güver, T., Wroblewski, P., Camarota, L., & Özel, F. 2010, *ApJ*, 719, 1807
- Haensel, P., Zdunik, J. L., & Schaefer, R. 1986, *A&A*, 160, 121
- Hendi, S. H., Bordbar, G. H., Eslam Panah, B., & Najafi, M. 2015, *Ap&SS*, 358, 7
- Hendi, S. H., Bordbar, G. H., Eslam Panah, B., & Panahiyan, S. 2016a, *J. Cosmol. Astropart. Phys.*, 9, 013
- Hendi, S. H., Faizal, M., Panah, B. E., & Panahiyan, S. 2016b, *European Physical Journal C*, 76, 296
- Hendi, S. H., Bordbar, G. H., Eslam Panah, B., & Panahiyan, S. 2017, *J. Cosmol. Astropart. Phys.*, 7, 004
- Herrera, L. 1992, *Physics Letters A*, 165, 206
- Katsuragawa, T., Nojiri, S., Odintsov, S. D., & Yamazaki, M. 2016, *Phys. Rev. D*, 93, 124013
- Knop, R. A., Aldering, G., Amanullah, R., et al. 2003, *ApJ*, 598, 102
- Lake, K. 2003, *Phys. Rev. D*, 67, 104015
- Maurya, S. K., Ray, S., Ghosh, S., Manna, S., & T. T., S. 2018, *Annals of Physics*, 395, 152
- Momeni, D., & Myrzakulov, R. 2015, *International Journal of Geometric Methods in Modern Physics*, 12, 1550014
- Narain, G., Schaffner-Bielich, J., & Mishustin, I. N. 2006, *Phys. Rev. D*, 74, 063003

- Oppenheimer, J. R., & Volkoff, G. M. 1939, *Physical Review*, 55, 374
- Paul, B. C., Chattopadhyay, P. K., Karmakar, S., & Tikekar, R. 2011, *Modern Physics Letters A*, 26, 575
- Perlmutter, S., Aldering, G., Goldhaber, G., et al. 1999, *ApJ*, 517, 565
- Rawls, M. L., Orosz, J. A., McClintock, J. E., et al. 2011, *ApJ*, 730, 25
- Riess, A. G., Filippenko, A. V., Challis, P., et al. 1998, *AJ*, 116, 1009
- Sharif, M., & Fatima, H. I. 2016, *International Journal of Modern Physics D*, 25, 1650083
- Shee, D., Deb, D., Ghosh, S., Ray, S., & Guha, B. 2018, *International Journal of Modern Physics D*, 1850089
- Sheykhi, A., Riazi, N., & Mahzoon, M. H. 2006, *Phys. Rev. D*, 74, 044025
- Silbar, R. R., & Reddy, S. 2004, *American Journal of Physics*, 72, 892
- Stergioulas, N. 2003, *Living Reviews in Relativity*, 6, 3
- Stuchlík, Z. 2000, *ACTA PHYSICA SLOVACA*, 50, 219
- Tolman, R. C. 1939, *Physical Review*, 55, 364
- Tonry, J. L., Schmidt, B. P., Barris, B., et al. 2003, *ApJ*, 594, 1
- Visser, M., & Barcelo, C. 2000, in *Cosmo-99* (World Scientific), 98
- Waga, I. 1993, *ApJ*, 414, 436
- Witten, E. 1984, *Phys. Rev. D*, 30, 272
- Zubairi, O., Romero, A., & Weber, F. 2015, *J. Phys. Conf. Ser.*, 615, 012003